arXiv:1702.06476v1 [physics.optics] 21 Feb 2017

Reconfigurable arbitrary nonreciprocal transfer functions through nonreciprocal coupling

Christopher W Peterson[1], Seunghwi Kim[2], Jennifer T Bernhard[1], and Gaurav Bahl[2,*]

[1]Electrical and Computer Engineering, University of Illinois at Urbana-Champaign
[2]Mechanical Science and Engineering, University of Illinois at Urbana-Champaign
[*]To whom correspondence should be addressed; bahl@illinois.edu

February 22, 2017

Abstract

Breaking reciprocity associated with wave propagation is a fundamental challenge across a wide range of physical systems in electromagnetics, optics, and acoustics. In contrast to established magneto-optic methods, recent efforts have focused instead on inducing nonreciprocity using time-varying biases such as synchronized spatiotemporal modulation of resonators and waveguides. To date, the elements that couple these time-varying resonator and waveguide modes are always considered to be reciprocal, and the nonreciprocal transfer functions achieved by these systems have been mostly limited to narrow-band resonances. Here we demonstrate that transferring the time-varying bias to the often overlooked coupling between waveguides and resonators can permit the synthesis of arbitrary nonreciprocal transfer functions. Using simple microwave circuits we experimentally demonstrate dynamically reconfigurable nonreciprocal responses, and the possibility of arbitrary function synthesis, through the use of this nonreciprocal coupler. This unique method of breaking reciprocity is applicable to essentially all wave phenomena, opening the door for the creation of a broad class of nonreciprocal systems.

Reciprocity is a fundamental property of wave propagation in linear time-invariant (LTI) media[1] that implies invariance of a system when its inputs and outputs are exchanged and arises due to the symmetry of the medium under time-reversal. In classical systems reciprocity is best captured through network theory, where a reciprocal network is defined by a symmetric scattering matrix $S = S^{T}$ [2,3]. The off-diagonal elements of this matrix describe the transmission of waves between any two ports of the network. Since the reciprocity property derives from time-reversal symmetric media, nonreciprocal networks can be created by applying a time-varying bias that generates the property $S_{mn}(\tau) \neq S_{mn}(-\tau)$, where τ is the time variable of the bias. Under such a bias the scattering matrix will become asymmetric and nonreciprocal, but will retain the property that $S_{mn}(\tau) = S_{nm}(-\tau)$. Historically, linear nonreciprocal networks have been predominantly based on the magneto-optic effect in gyrotropic materials[4,5] and can be understood by the relationship[6] $S_{mn}(\vec{H}) = S_{nm}(-\vec{H})$ under influence of magnetic field $\vec{H}$. Magnetically induced nonreciprocity may be also considered a subset of the time-variation approach since magnetic fields are quantifiable by the time parameter of an equivalent current loop.

Recent efforts on achieving linear nonreciprocal effects without magnetic fields have focused on using spatiotemporal biases in optical, RF, and acoustic domains[7–21]. For instance, the scattering of light from a propagating acoustic wave in a medium depends on the relative momentum vectors of the photons and phonons and the available density of states in each domain. Such a traveling

acoustic wave bias can thus be exploited to generate nonreciprocal effects[17,18]. Most systems of this type can be generalized to a combination of ports, waveguides, and resonances (Fig. 1**a**). Generally, we can describe these systems using coupled mode theory through the equations[22–24]

$$\dot{\alpha} = (j\Omega - \Gamma)\alpha + D^T a \ , \tag{1}$$

$$b = Ca + D\alpha \ , \tag{2}$$

where $\alpha,\ a,\ b$ are complex valued vectors respectively describing the field in the resonances, into the ports, and out of the ports as illustrated. Four matrices, $\Omega,\ \Gamma,\ D,\ C$, represent the system parameters: resonance frequencies, resonance decay rates, coupling between the ports and the resonances, and coupling between ports respectively. The scattering matrix S, which is only dependent on the four matrices that describe the system, can be obtained through the relationship $b = Sa$. Past research has shown that a nonreciprocal (asymmetric) scattering matrix can be obtained by applying a spatiotemporal bias to coupled resonant modes ($\Omega,\ \Gamma$ matrix)[13,19] or the waveguide (C matrix)[7,16] but the coupling between these waveguides and resonances (D matrix) is always assumed to be linear time invariant.

In this work, we invert the situation and demonstrate instead an approach to achieving nonreciprocal propagation in LTI waveguides and resonators through the use of spatiotemporally modulated coupling (D matrix) while keeping resonances and waveguides unchanged. As we will show, the power of using this approach is that highly tailorable nonreciprocal transfer functions can be arranged without needing sophisticated modulation schemes involving multiple synchronized resonances or waveguides[10,13,16,19]. The use of nonreciprocal coupling also opens new and convenient paths to produce a variety of nonreciprocal devices using a single waveguide and resonator. We discuss how ultra low loss isolators could be created through nonreciprocal critical coupling and gyrators (nonreciprocal phase-shifters) could be created nonreciprocal over-coupling to resonators.

In this paper we first develop a theory for directly generating a nonreciprocal coupling matrix D using spatiotemporally modulated coupling elements. Using this approach, we experimentally demonstrate significant nonreciprocal responses in simple resonant microwave circuits. We discuss how nonreciprocal coupling automatically creates networks that are theoretically lossless in the uncoupled direction and how it can be applied to arbitrary resonant structures and impedance networks.

1 Results

1.1 Nonreciprocal coupling via multiple reciprocal couplers

Let us consider a system consisting of a waveguide connecting 2 ports as illustrated in Fig. 1b. A resonator supporting a mode with frequency ω_0 is coupled to this waveguide at N independent coupling points, such that each coupler is spatially separated on the waveguide by an identical length ℓ. For simplicity, we assume that these couplers are all connected to the resonator at antinodes of equal phase for the resonant mode at ω_0. Using the framework of temporal coupled mode theory[22–24], we will first derive an effective coupling coefficient for this system, and we will show later that the effective coupling is sensitive to the direction of wave propagation when spatiotemporal modulation is applied to the individual coupling coefficients. The use of coupled mode theory generalizes the analysis allowing for implementation with electromagnetic, optical, or acoustic waves without changing the underlying systemic principles.

We can describe the complex-valued excitation amplitude α of the resonant standing wave mode (traveling modes are discussed in the Supplementary Information section S1) through equation (1),

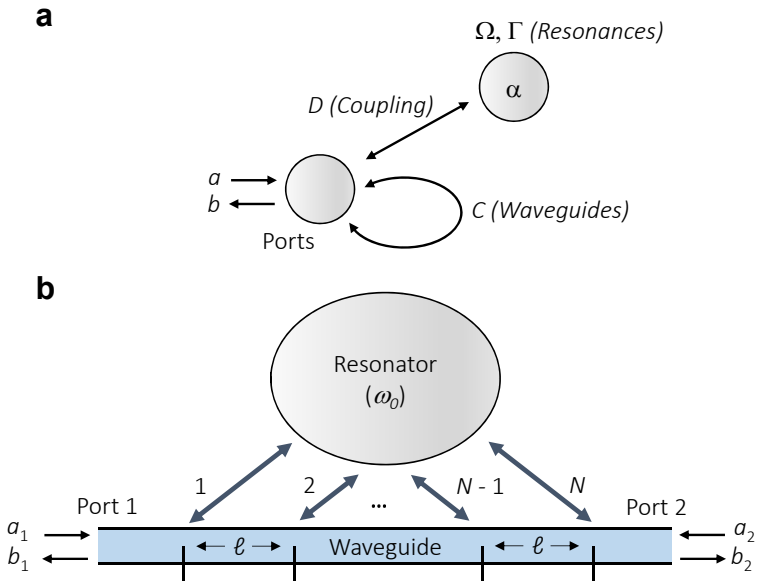

Figure 1: **a** Schematic representation of a general waveguide-resonator system. Ports are coupled directly via waveguides described by the scattering matrix C, and can also couple to resonant modes via the coupling matrix D. The inputs and outputs at the ports are described by the vectors a and b respectively. The resonant field vector α is described through the frequency matrix Ω and the decay matrix Γ. **b** In a simple system with one resonance and two ports, nonreciprocity can be synthesized through the coupling matrix D using a system of N spatiotemporally modulated capacitive couplers. The individual couplers are spatially distributed over the waveguide with subwavelength spacing ℓ in order to generate sensitivity to wave propagation direction. For mathematical simplicity, we assume that each coupler is connected to an isophase point of the resonant mode. Sinusoidal time-modulation of the individual coupling rates at a relative phase set by their spatial location generates significant nonreciprocal effects that we see in this work.

$$\dot{\alpha} = (j\omega_0 - \gamma)\alpha + D_1 a_1 + D_2 a_2 \ , \tag{3}$$

where ω_0 and γ describe the frequency and decay rate of the resonance, and ω is the analysis frequency of the waves traveling into the ports. Waves incident on port 1, described by a_1, are coupled to the resonator with effective coupling D_1, which is the sum of contributions from all N couplers

$$D_1 = \sum_{n=1}^{N} j d_n e^{-j\beta\ell(n-1)} \ . \tag{4}$$

Here d_n describes the coupling strength of the n^{th} coupler, numbered such that d_1 is nearest to port 1 and d_N is nearest to port 2. Waves incident on port 2 (a_2) are likewise coupled to the resonator through the effective coupling strength

$$D_2 = \sum_{n=1}^{N} j d_n e^{j\beta\ell(n-N)} \ . \tag{5}$$

We here assume that losses in the waveguide can be neglected and propagation is solely described by the waveguide phase constant β. In general, the spatial separation of the multiple couplers causes the effective couplings D_1 and D_2 to be sensitive to the direction of wave propagation. Although this directional sensitivity does not in general lead to nonreciprocity, it is a crucial part of the nonreciprocal coupling theory that we develop in this paper. As a practical consideration we note

that the waveguide propagation constant β will be a function of frequency due to the waveguide dispersion, and will result in some deviation from this theory. For simplicity we will ignore the effects of waveguide dispersion.

For a 2-port system to be nonreciprocal it is sufficient that the transmission coefficients S_{21} and S_{12} are not equal. These steady-state transmission coefficients are defined as $S_{21} = b_2/a_1$ (with $a_2 = 0$) and $S_{12} = b_1/a_2$ (with $a_1 = 0$) where b_2 and b_1 (the outgoing wave amplitudes at port 2 and port 1) are defined by equation (2)

$$\begin{aligned} b_2 &= e^{-j\beta\ell(N-1)}a_1 + D_2\alpha \ , \\ b_1 &= e^{-j\beta\ell(N-1)}a_2 + D_1\alpha \ . \end{aligned} \tag{6}$$

For the simple case where each coupler has the same coupling strength $d_n = d_0$, we can find a compact form of the transmission coefficients

$$S_{21} = S_{12} = e^{-j\beta\ell(N-1)}\left[1 - \frac{d_0^2 N^2 H_N(\beta\ell)}{j(\omega-\omega_0)+\gamma}\right] , \tag{7}$$

where we have introduced a dimensionless periodic function $H_N(\theta)$ that describes the squared efficiency of the effective coupling. $H_N(\theta)$ is defined as

$$H_N(\theta) = \frac{1}{N^2}\left|\sum_{n=1}^{N} e^{-j\theta n}\right|^2 , \tag{8}$$

and is described in detail in the Supplementary Information. This function is symmetric about $\theta = n\pi$ and periodic such that $H_N(\theta) = H_N(\theta + 2n\pi)$ for integer n, and concisely describes the effective excitation of the resonant mode resulting from interference due to the multiple couplers. The zeros of $H_N(\theta)$ arise when the interference is completely destructive (i.e. the resonator and waveguide are phase mismatched) and the resonant mode is not excited at all. Note that the resonator decay rate γ can be defined as[24]

$$2\gamma = \langle D_1 D_1^* + D_2 D_2^* + \kappa_i \rangle \tag{9}$$

where $\langle\ \rangle$ denotes the time-average. Therefore γ can also be expressed in terms of $H_N(\beta\ell)$, making the efficiency function extremely useful in simplifying the system equations. Here κ_i describes the intrinsic decay rate of the resonator.

Let us now consider the case where the coupling strength at each individual coupling point is sinusoidally modulated with amplitude d_M and frequency Ω around a static value d_0, where $\omega_0 >> \Omega >> \gamma$. Additionally, we apply a discretely spaced phase shift $-n\phi$ to the modulation term for the $(n+1)^{th}$ coupler such that $d_n = d_0 + d_M \cos\big(\Omega\tau - \phi(n-1)\big)$. This phase shift creates a discretized traveling modulation wave, or in other words a 'synthetic phonon' having a wave-vector controlled by the relative phase ϕ. We can apply this spatiotemporally varying coupling to equations (1, 2) to find the steady-state transmission coefficients

$$\begin{aligned} S_{21} = \Bigg[1 &- \frac{d_0^2 N^2 H_N(\beta\ell)}{j(\omega-\omega_0)+\gamma} - \frac{1}{4}\frac{d_M^2 N^2 H_N(\beta\ell+\phi)}{j(\omega+\Omega-\omega_0)+\gamma} \\ &- \frac{1}{4}\frac{d_M^2 N^2 H_N(\beta\ell-\phi)}{j(\omega-\Omega-\omega_0)+\gamma}\Bigg] e^{-j\beta\ell(N-1)} \ , \text{ and} \end{aligned} \tag{10}$$

$$S_{12} = \Bigg[1 - \frac{d_0^2 N^2 H_N(\beta\ell)}{j(\omega-\omega_0)+\gamma} - \frac{1}{4}\frac{d_M^2 N^2 H_N(\beta\ell-\phi)}{j(\omega+\Omega-\omega_0)+\gamma} - \frac{1}{4}\frac{d_M^2 N^2 H_N(\beta\ell+\phi)}{j(\omega-\Omega-\omega_0)+\gamma}\Bigg] e^{-j\beta\ell(N-1)}. \tag{11}$$

Equations (10, 11) define transmission for incident and outgoing waves of the same frequency ω and do not explicitly describe outgoing waves at other frequencies. Recalling from equation (9) that γ is dependent on the squared magnitude of the effective coupling we note that resonator decay rate will increase when this type of modulation is applied, which is in fact required for energy conservation.

The above transfer functions reveal distinct transmission dips at the original resonance ω_0 and at sidebands $\omega_0 \pm \Omega$. Notably, in the sidebands the $H_N(\theta)$ function is offset by the modulation phase difference ϕ, with the sign of this offset determined by the direction of wave propagation in the waveguide. In the general case we have $H_N(\beta\ell+\phi) \neq H_N(\beta\ell-\phi)$ implying that the sideband transmission coefficients S_{21} and S_{12} are unequal and the system is nonreciprocal. This nonreciprocity condition is always satisfied if neither $\beta\ell$ nor ϕ is an integer multiple of π. The induced nonreciprocity in this system is clearly of the canonical form $S_{21}(\tau) = S_{12}(-\tau)$, since a transformation of $\tau \to -\tau$ is equivalent to $\phi \to -\phi$ in the equation for d_n.

Figure (2) shows theoretically calculated transmission at the upper sideband frequency $\omega_0 + \Omega$ for systems having two and three couplers ($N = 2, 3$), corresponding to the simplest possible implementations. The transmission at the lower sideband can be found by simply reversing the sign of ϕ, as seen in equations (10, 11). This figure is simplified such that β does not vary with frequency, a useful approximation if the variation is small over the desired frequency range. We find that the largest transmission dips are centered on the zeros of $H_N(\beta\ell)$, i.e. the values of $\beta\ell$ where the original resonant mode at ω_0 is totally uncoupled from the waveguide. The sidebands can still couple at these points with a coupling efficiency described by $H_N(\beta\ell \pm \phi)$, but the overall decay rate of the mode (γ) is minimized because there is no decay at the center frequency. The minimized decay rate means the quality-factor of the resonance is maximized and the dip is transmission as deep and narrow as possible. By extension of this idea, for a given sideband coupling rate the transmission dip in that sideband will increase in depth and decrease in width as coupling to the original resonance decreases.

Figure 2 illustrates that for the $N = 2$ system the maximum transmission dip occurs at $\beta\ell = \pi$, a symmetry point of H_N that unfortunately exhibits a reciprocal transmission response. This symmetry problem is easily overcome in a $N > 2$ system, since zeros of H_N will then occur away from $\beta\ell = \pi$. Notably, for $N = 3$ the transmission is maximally nonreciprocal for $\beta\ell = \pm 2\pi/3$ and a relative phase setting of $\phi = \pm 2\pi/3$. We additionally note that more couplers will also increase the total effective coupling to the mode as evidenced by the N^2 term in equations (10, 11), implying greater transmission contrast if implemented.

We note that the derivation presented here describes a standing wave resonator, where incident waves from both ports are coupled to the same resonant mode. As we discuss in the Supplementary Information, the method we propose for creating nonreciprocal transmission can also be applied to a traveling wave resonator having intrinsic directionality to its resonant modes. In fact, since the effective coupling itself is direction sensitive, our approach is generally independent of the type of resonator used. However, care must be taken when using a standing wave resonator since simultaneous incident waves from both ports can interfere in the resonator. This problem is automatically resolved if waves in one direction are completely uncoupled from the resonance, which

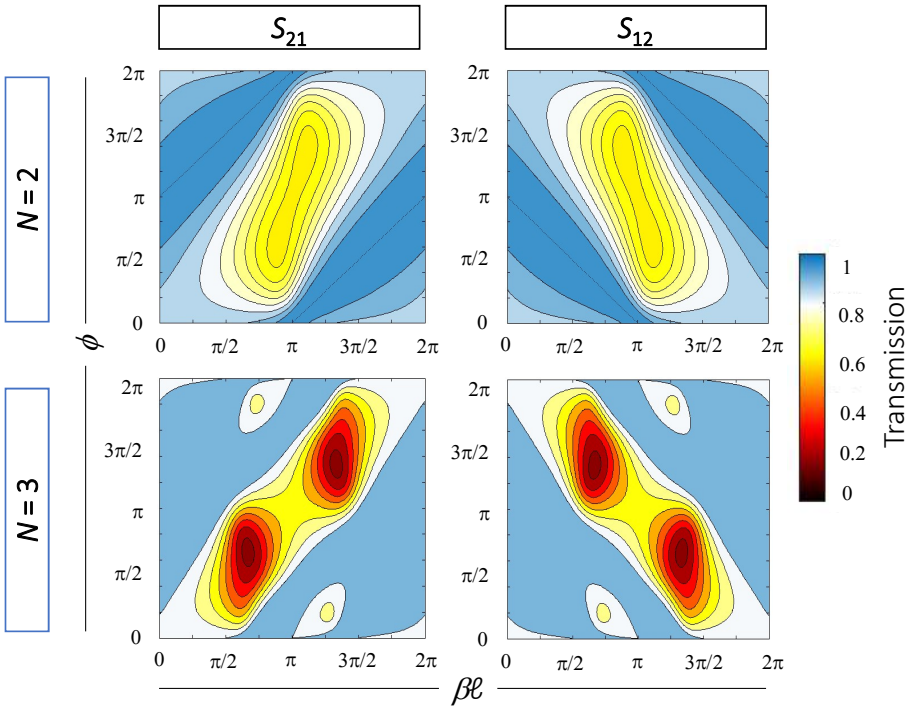

Figure 2: Calculated waveguide transmission coefficient magnitudes (equations (10, 11)) through the system of Fig. 1**b** at the upper sideband frequency $\omega_0 + \Omega$, where Ω is the frequency of the applied coupler modulation. Rows indicate the case of two ($N = 2$) and three ($N = 3$) coupling points, corresponding to the simplest possible implementations of nonreciprocal coupling. For each figure, the x-axis represents the phase-separation ($\beta\ell$) between adjacent couplers, while the y-axis represents the relative phase setting (ϕ) of the applied modulation at each coupler. In a typical system $\beta\ell$ will correspond to the physical design while ϕ is a dynamically adjustable parameter. Low transmission corresponds to stronger coupling, since the incoming waves are absorbed by the resonator. As anticipated, the effective total coupling differs for forward (S_{21}) and backward (S_{12}) propagating waves. The transmission coefficients are mirrored about $\phi = \pi$, demonstrating the relationship $S_{21}(\tau) = S_{12}(-\tau)$. Large contrast can be achieved in a system of 3 coupling points designed with $\beta\ell = 2\pi/3$ having a relative phase setting of $\phi = \pm 2\pi/3$.

is also necessary for a maximum nonreciprocal response and lossless propagation in the uncoupled direction.

1.2 Lossless device design

A common goal of nonreciprocal networks is to create a strong directional effect, such as complete isolation or a unidirectional phase-shift. In order to create these effects through nonreciprocal coupling, it is useful if waves propagating in one direction are strongly coupled to the resonant mode while counter-propagating waves are completely uncoupled. This special case occurs when $H_N(\beta\ell + \phi) = 0$ and $H_N(\beta\ell - \phi) = 1$, and when applied to equations (10, 11) we see that transmission in the uncoupled direction becomes lossless ($|S_{mn}| = 1$). For example, this occurs for $N = 3$ when $\beta\ell = \phi = 2\pi/3$ (see Fig. S2 in the Supplementary Information). When the additional condition that $\gamma = \frac{1}{4} d_M^2 N^2 H_N(\beta\ell - \phi)$ is met the system is critically coupled and behaves as an ideal isolator at the sideband frequency, with unity transmission magnitude in one direction and no transmission in the other. Note that is also applies if the sign of ϕ is flipped.

A network that imparts a unidirectional π phase-shift, often called a gyrator, is an important

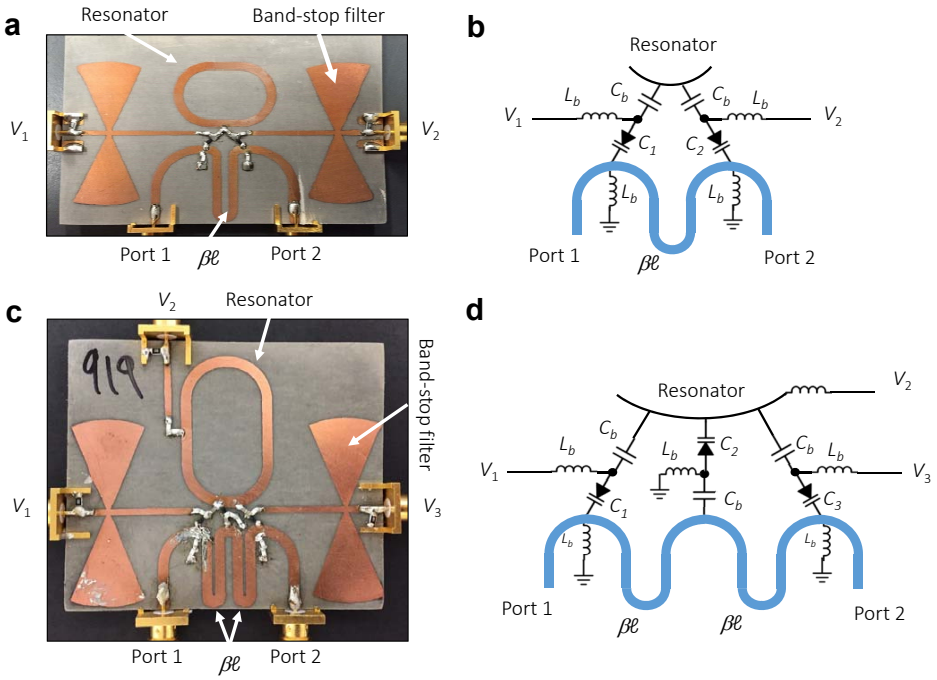

Figure 3: Microwave demonstration circuits for reconfigurable nonreciprocal coupling. a, b Photograph and schematic of a system with $N = 2$ coupling points. **c, d** Photograph and schematic of a system with $N = 3$ coupling points. Each microstrip ring resonator is coupled to the waveguide through multiple varactor diodes that are separated on the waveguide by phase $\beta\ell$, with the dc and time-modulated biased controlled using voltages V_n. For the 3-coupler circuit, biasing to the central varactor is provided through the resonator.

nonreciprocal component that can be used to create circulators and more complex nonreciprocal circuits. Our system can behave as a gyrator if certain conditions are met. Specifically, waves from one direction must be uncoupled from the resonance while counter-propagating waves are strongly coupled at one of the sidebands ($H_N(\beta\ell + \phi) = 0$ and $H_N(\beta\ell - \phi) = 1$). Simultaneously, waves traveling in both directions must be uncoupled at the original resonance and the other sideband. This can be achieved with a waveguide that is dispersive or has a bandgap. In this configuration an ideal gyrator can be approached as $\gamma \to \frac{1}{8} d_M^2 N^2 H_N(\beta\ell - \phi)$. The conditions leading to ideal isolation and gyration are thus fundamentally possible to achieve with careful system engineering, allowing our simple nonreciprocally coupled waveguide-resonator system to be used as a building block for more complex nonreciprocal circuits.

1.3 Experimental Results

We implemented nonreciprocal waveguide-resonator systems having $N = 2$ and $N = 3$ couplers using microwave frequency microstrip circuits[25], shown in Fig. 3. We also introduce a time-modulated coupling with controllable phase shift at each coupling point in order to generate the requisite 'synthetic phonon' wave (see Methods).

The fabricated resonator system with two couplers ($N = 2$) shown in Fig. 3**a,b** has a loaded resonance frequency $\omega_0/2\pi \approx 1.57$ GHz. Figure 4**a** shows the measured lower and upper transmission sidebands in forward and reverse directions when $\Omega/2\pi = 100$ MHz modulation is applied to the couplers, with relative phase setting of $\phi = 0$ (dashed lines) and $\phi = \pi/2$ (solid lines). In Fig-

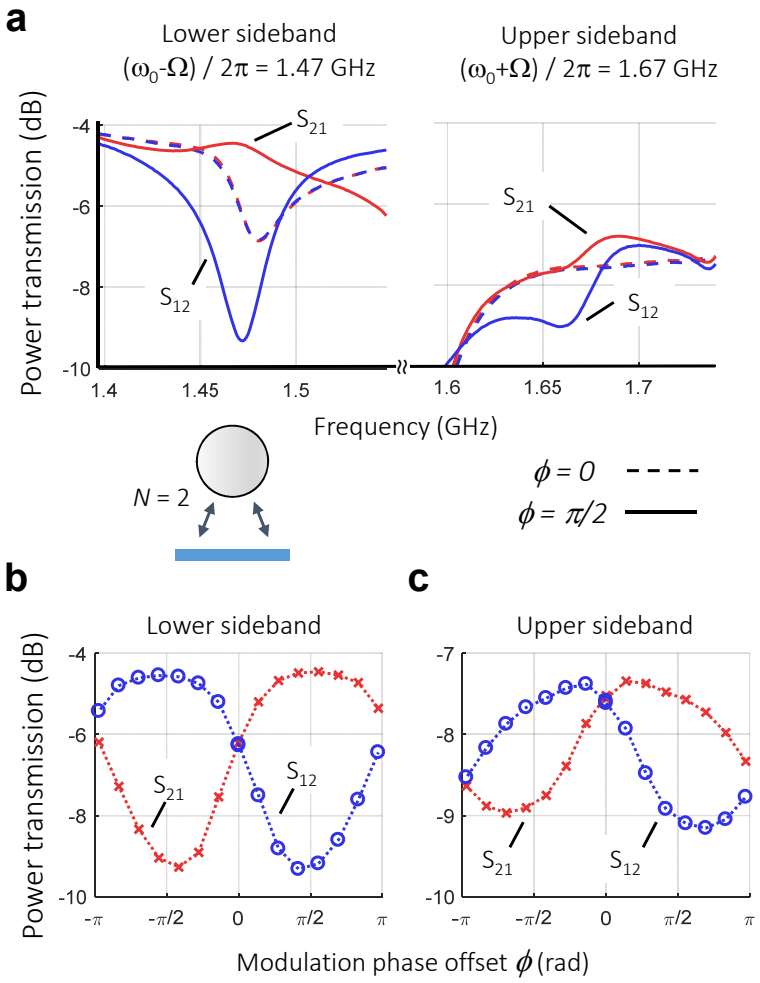

Figure 4: **a** Experimentally measured power transmission coefficients for the $N = 2$ circuit are presented at both sidebands using 100 MHz modulation applied to the couplers. Data for forward transmission (S_{21}, red) and backward transmission (S_{12}, blue) are presented for both $\phi = 0$ (dashed lines) and $\phi = \pi/2$ (solid lines). **b,c** Data present the line-center forward (red, x) and backward (blue, o) transmission coefficients at the lower (upper) sideband frequency 1.47 GHz (1.67 GHz) for selected values of ϕ. We observe nonreciprocal coupling to the resonance while using coupler phase settings of $\phi \neq 0, \pi$ in both upper and lower sidebands of the resonance.

ure 4**b,c** we quantify the measured transmission at the lower sideband resonance (frequency $\omega_0 - \Omega$) and upper sideband resonance ($\omega_0 + \Omega$) respectively, as ϕ is swept from $-\pi$ to π. As predicted, we observe reciprocal transmission at $\phi = 0,\ \pi$. However, when ϕ is not equal to an integer multiple of π the coupling in the sidebands diverges depending on wave directionality, resulting in appreciable nonreciprocal transmission. In the lower sideband there is minimum forward coupling at $\phi = \pi/2$ and minimum reverse coupling at $\phi = -\pi/2$, confirming that the fabricated circuit has $\beta\ell = \pi/2$ at the lower sideband $\omega = \omega_0 - \Omega$. On the other hand, we see that upper sideband coupling is minimized at $\phi \approx \pm\pi/6$ (positive sign corresponds to minimized forward coupling) indicating that $\beta\ell = 7\pi/6$ at $\omega = \omega_0 + \Omega$. The large difference in $\beta\ell$ for these two frequencies can be attributed to the dispersion characteristics of the waveguide which are non-negligible in our experiment. We additionally note that the upper sideband is much smaller and misshapen compared to the lower sideband, which is due to additional undesired resonant modes and reflections in our circuit imple-

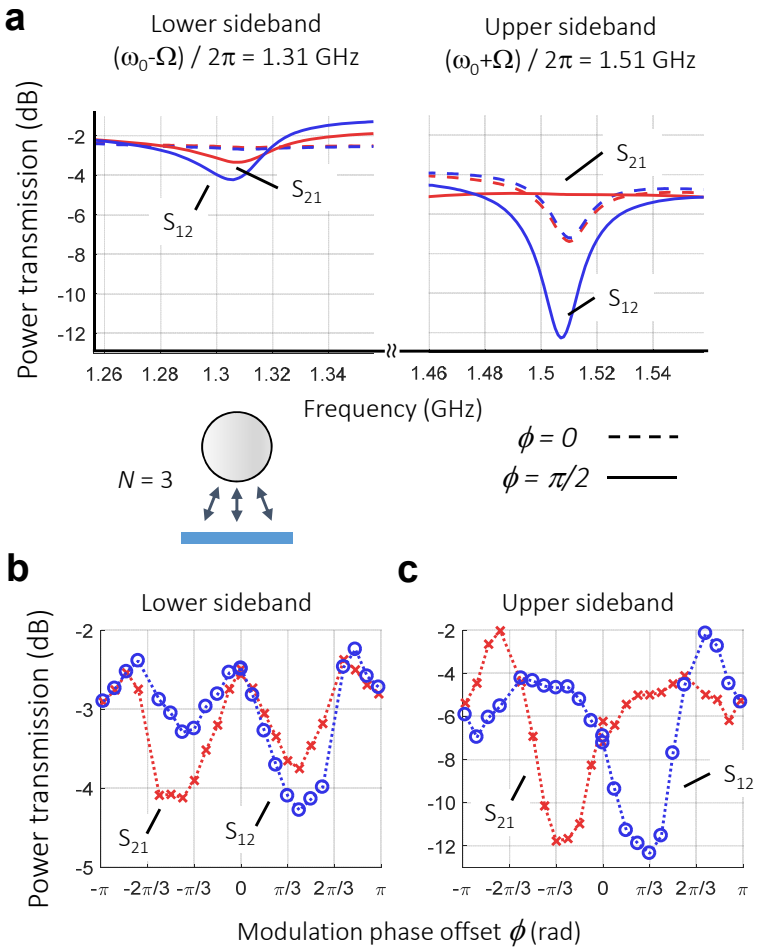

Figure 5: **a** Experimentally measured power transmission coefficients for the $N = 3$ circuit are presented at both sidebands using 100 MHz modulation applied to the couplers. Data for forward transmission (S_{21}, red) and backward transmission (S_{12}, blue) are presented for both $\phi = 0$ (dashed lines) and $\phi = \pi/3$ (solid lines). **b,c** Data present the line-center forward (red, x) and backward (blue, o) transmission coefficients at the lower (upper) sideband frequency 1.31 GHz (1.51 GHz) for selected values of ϕ. Again we observe nonreciprocal coupling when $\phi \neq 0, \pi$.

mentation. Despite these experimental difficulties, we observe strong nonreciprocal coupling and over 5 dB of directional contrast in this initial experiment.

Our test system with three coupling points ($N = 3$) has a loaded resonance frequency $\omega_0/2\pi \approx 1.41$ GHz and is presented in Fig. 3**c,d**. Figure 5**a** shows the lower and upper sideband measurements for $\phi = 0$ (dashed lines) and $\phi = \pi/3$ (solid lines) for an applied modulation frequency of $\Omega/2\pi = 100$ MHz. In Fig. 5**b,c** we present the measured transmission at the lower and upper sideband resonances as ϕ is swept from $-\pi$ to π. As predicted in Fig. 2, this three coupler case yields two distinct dips in transmission (one large, one small) as the phase setting ϕ is varied. These two dips in transmission correspond to two local maximums in the coupling efficiency function H_3. In the lower sideband the large transmission dip occurs at $\phi \approx \mp\pi/3$ (minus sign corresponding to minimized forward transmission) corresponding to $\beta\ell = \pi/3$. Figure 5**a** shows simultaneous coupling of both forward and backward waves to the resonance at the lower sideband. This occurs since forward waves couple to the resonator due to the small local maximum of $H_N(\beta\ell + \phi)$, while backward waves couple strongly at the large local maximum. These two local maxima occur

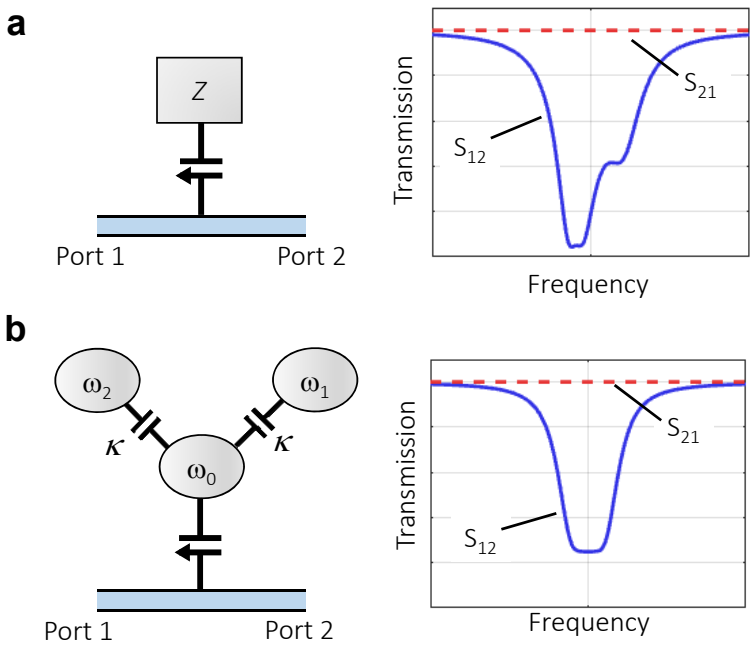

Figure 6: Nonreciprocal couplers enable the generation of arbitrary transfer functions: a An impedance Z that is nonreciprocally coupled to a waveguide can generate an elaborate nonreciprocal transfer function. The capacitor with an arrow is used here as a symbol representing nonreciprocal coupling which only couples waves traveling in the direction of the arrow. **b** A flatband nonreciprocal band-pass filter can be easily produced using three resonators and one nonreciprocal capacitive coupler. The simulated S_{12} curve is evaluated with $\omega_1 = \omega_0 - \frac{3}{7}\gamma_0$, $\omega_2 = \omega_0 + \frac{3}{7}\gamma_0$, $\gamma_1 = \gamma_2 = \gamma_0$, $\kappa = \frac{9}{14}\gamma_0$. Here, γ_n is the decay rate associated with the n^{th} resonator and κ is the coupling rate between the resonators.

for the same modulation phase ϕ due to the waveguide dispersion. The upper sideband exhibits similar behavior with one large local coupling maximum at $\phi = \mp\pi/3$ and a smaller local coupling maximum at $\phi \approx 4\pi/3$, corresponding to $\beta\ell = 5\pi/3$. Again, this large difference in $\beta\ell$ between the sidebands can be attributed to non-idealities in the circuit implementation. Figure 5**c** shows that on the upper sideband we are able to achieve strong coupling for backward waves and essentially zero coupling for forward propagating waves, demonstrating over 7 dB of contrast with $\phi = \pm\pi/3$.

1.4 Generation of arbitrary nonreciprocal transfer functions

A key advantage of employing generalized nonreciprocal couplers is that the nonreciprocal transfer function is not limited to the response of simple resonator. This possibility arises since the shape of the transfer functions S_{21} and S_{12} are determined by the denominator of equations (10, 11), while the nonreciprocity generated by the coupling, is contained within the numerator. To illustrate, let us consider an arbitrary shunt impedance that is coupled capacitively to a waveguide and generates an elaborate transfer function, such as that of a multi-band filter. Use of a nonreciprocal coupler instead of the linear coupler between the waveguide and this shunt impedance will cause the transfer function to appear only for reverse propagating waves at the sideband frequencies as illustrated in Fig. 6**a**. A specific example that can be generated using an impedance composed of only a few coupled resonators is a nonreciprocal band-reject filter, as illustrated in Fig. 6**b**. This capability has not been demonstrated in other approaches to creating nonreciprocal responses, as many of these approaches rely on exact resonance conditions[13,17,19,20] and do not allow for arbitrary impedance networks.

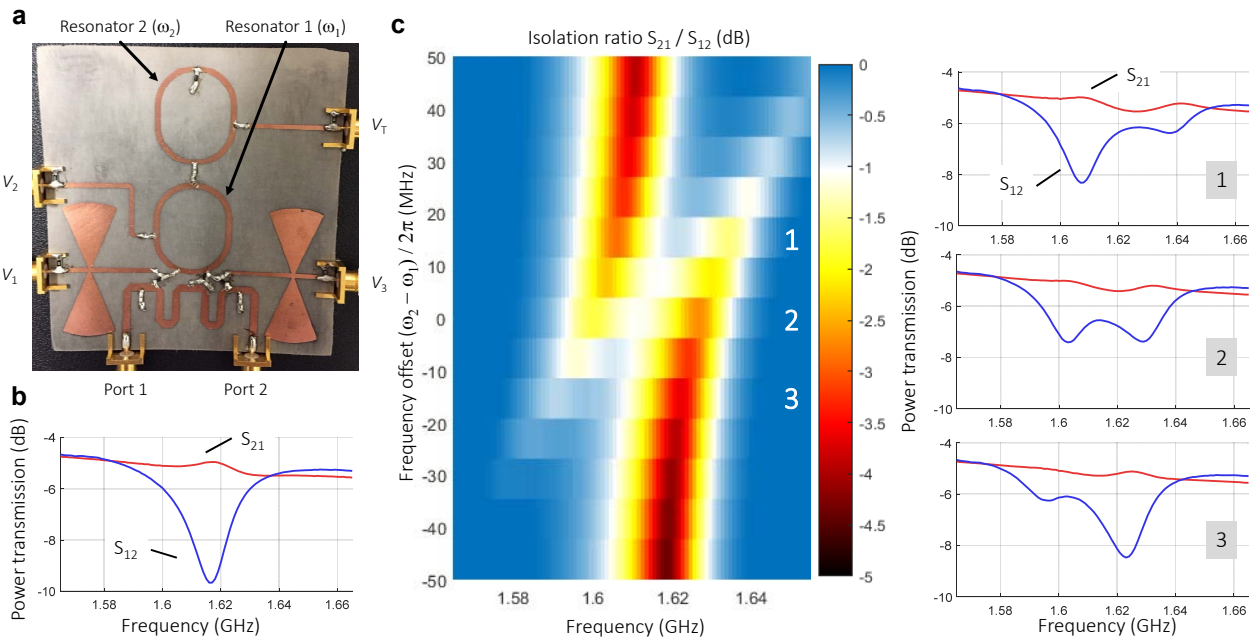

Figure 7: **a** Photograph of a $N = 3$ circuit used to demonstrate nonreciprocal coupling to a split resonance. The circuit is functionally identical to the previous experiment except for an additional resonator coupled to the first. An applied voltage V_T is used to tune the center-frequency of the second resonance. **b** Measured nonreciprocal transmission coefficients S_{21} (red) and S_{12} blue at the upper sideband ($(\omega_0 + \Omega)/2\pi \approx 1.62$ GHz) when the resonance frequencies of the coupled resonators are far apart, similar to previous experiments. **c** Measured isolation ratio and transmission coefficients (numbered 1-3) at the upper sideband when the second resonance (ω_2) is tuned across the first (ω_1). We observe that backward propagating waves couple effectively to the split resonance in this sideband although both modes are at a much lower frequency, clearly demonstrating that the nonreciprocity is caused by the modulated coupling. An increase in the directional contrast (isolation) bandwidth due to the broadening of the mode is also evident.

To experimentally verify this concept of nonreciprocal coupling to an arbitrary resonant state, we produced the simple two-resonator circuit shown in Fig. 7**a**. This microwave circuit is a direct extension of the $N = 3$ implementation (Fig. 3**c,d**) in which a second resonator (ω_2) has been coupled to the first resonator (ω_1) through a fixed capacitor. The resonance frequency of this added resonator can be capacitively tuned using a voltage controlled varactor diode at the top of the ring. The nonreciprocal coupler placed between the waveguide and resonator is modulated using $\Omega/2\pi = 100$ MHz with a phase setting of $\phi = \pi/3$. Figure 7**b** presents the measured nonreciprocal coupling occurring between the first resonator and the waveguide at the upper sideband frequency $(\omega_1 + \Omega)/2\pi \approx 1.61$ GHz, when the frequencies of the two coupled resonances are far apart. The second resonance at ω_2 is then tuned across the first resonance at ω_1, resulting in an avoided crossing and lifted degeneracy of the hybrid modes of the system. The avoided crossing is easily observed in our measurements of the S_{21}/S_{12} isolation contrast in Fig. 7**c** at the sideband frequency. This simple example showcases that nonreciprocal transfer functions that are more complex than simple resonances[7,9–21] can be obtained quite readily by this approach.

2 Discussion

In this study we have presented a theoretical description and experimental validation of employing multiple spatiotemporally modulated couplers to create nonreciprocal coupling in a very simple 2-port system. We have also discussed how such a system could theoretically achieve unidirectionally lossless nonreciprocal transmission, as well as how nonreciprocal coupling could be used to create arbitrary nonreciprocal transfer functions. The methods presented are independent of the type of resonator used and may be applied more broadly to optical and mechanical systems.

Presently, we were unable to observe lossless nonreciprocal transmission due to several non-ideal factors in the design. Specifically, in circuit implementation of a waveguide and ring resonator coupled with discrete capacitors there are several effects that are not accounted for in the temporal coupled-mode theory the most important of which are reflections from the capacitive couplers that can significantly distort the resonance shape and the slightly non-linear response of the varactor diodes. Due to this effect we observe scattering from the modulated couplers even far from the resonance, which effectively creates extra loss in the system. This behavior could be overcome in circuit implementations by lowering the intrinsic losses in the resonator and using a smaller capacitance for coupling. These modifications will decrease the distortion of the resonance shape as well as the non-linearity introduced by the varactor diodes.

Many experiments on nonreciprocal systems created through spatiotemporal modulation [9–12,15–18,26] can be seen through the lens of unidirectional inter-modal scattering or a momentum bias applied to the medium [7]. It is also possible to relate our work to this concept, with the momentum bias applied to the coupling coefficients instead of the waveguide or resonator components. However, major features of our demonstrated approach are that it allows the modulated region to be sub-wavelength, and that high-quality conventional (static) waveguides and resonators can be employed without the complexities of time-modulation. Further, the addition of a lossy element (the resonant mode) enables true signal isolation functionality where waves incident in one direction are dissipated as heat. Most importantly, we have experimentally demonstrated that nonreciprocal coupling enables the synthesis of arbitrary nonreciprocal transfer functions using conventional components and enables the use of well-known impedance networks. Such design capability has not been previously achieved in other approaches since they are often limited to exact resonant responses. Nonreciprocity achieved through nonreciprocal coupling is thus a powerful technique that can offer greater reconfigurability and customization of the system dynamics and signal processing functions.

3 Methods

3.1 Experimental Setup

Our microwave circuits are fabricated on Rogers 6006 substrate with a 1oz copper conductor, and consist of a microstrip waveguide coupled to a ring resonator by N varactor diodes (Skyworks SMV1275) that act as variable capacitors. The coupling strength d_n of each capacitive coupler is an approximately linear function of the applied voltage V_n for small changes in voltage, allowing a modulation of d_n that is proportional to a modulation of V_n. We first apply a DC bias of 3 volts to each varactor diode with a DC power supply (Agilent E3631A). We modulated this bias using a sine-wave from a signal generator (HP-8647B), which is set at a frequency of 100 MHz and a signal amplitude of 2 volts. The signal is split (Minicircuits ZA3CS-400-3W-S) into three lines that each connect to a variable phase shifter (Minicircuits JSPHS-150+) so that the phase shift between each signal can be independently controlled. After the splitting and taking into account the loss of the phase shifters and cables, we estimate about 1 volt AC bias at 100 MHz is applied to each varactor

diode. The DC bias and 100 MHz modulation are combined through a bias tee (Minicircuits ZFBT-4R2GW-FT+) connected directly to the circuit. On each circuit, butterfly band-pass filters were incorporated along with a another low-frequency biasing tee (Johanson Technology L-14C10N-V4T 10 nH inductor and Johanson Technology R14S 12 pF capacitor) as shown in Fig. 3 to isolate the lower frequency bias modulation from the higher frequency resonant circuit.

3.2 Modulation of the coupler elements

The applied 3 volt DC bias results in an average varactor capacitance of 1.87 pF, which is then modulated by the 1 volt AC signal from 1.58 pF to 2.32 pF. This is a slightly nonlinear voltage-capacitance relationship, but the non-linearity is small enough to not drastically impact the results. For large modulation amplitude we observed a shift in the phase ϕ at which the maximum and minimum coupling occur, due to interference between the applied biases and non-linearity in the phase shifters.

3.3 Measurement

We measured the transmission parameters (S_{21}, S_{12}) of the circuit using a Keysight E5063A vector network analyzer. The network analyzer measurement was calibrated to the ends of the SMA cables that connected to the surface-mount SMA connectors on the circuit board. Thus, the data presented throughout this paper only reflect the S parameters of the circuits that we have developed, while eliminating any parasitic effects from the cables and supporting systems.

4 Acknowledgments

We acknowledge funding support from the US Office of Naval Research (grant N00014-16-1-2830), the National Science Foundation Emerging Frontiers in Research and Innovation NewLAW program (grant EFMA-1627184), and a National Science Foundation Graduate Research Fellowship.

5 Author Contributions

C.W.P. and G.B. conceived the idea and with S.K. developed the theory. C.W.P. designed and carried out the experiments. J.T.B. provided material support and guidance for the experiments. All authors analyzed the data and co-wrote the paper. G.B. supervised all aspects of this project.

Supplementary Information

In this supplement we explicitly derive the nonreciprocal scattering parameters for a simple waveguide-resonator system with multiple spatiotemporally modulated couplers. The system under consideration, shown in Figure S1, consists of two ports connected by a waveguide with input and output fields described by a_m and b_m (where m is the port number) and a resonant mode with angular frequency ω_0 and amplitude α.

S1 Derivation of steady-state transmission coefficients

The mathematical derivations in this paper are an extension of temporal coupled-mode theory [24] modified to incorporate time-varying couplers. We begin with the differential equation describing the resonant field α of a standing-wave resonator in the time-domain with inputs a_1 and a_2 that are time-harmonic with frequency ω.

$$\dot{\alpha} = (j\omega_0 - \gamma)\alpha + D_1 a_1 + D_2 a_2 \ . \tag{S1}$$

This equation can be modified for a traveling wave resonator by simply splitting α into two orthogonal modes which are each only coupled to a single port.

$$\begin{aligned} \dot{\alpha_1} &= (j\omega_0 - \gamma)\alpha_1 + D_1 a_1 \ , \\ \dot{\alpha_2} &= (j\omega_0 - \gamma)\alpha_2 + D_2 a_2 \ . \end{aligned} \tag{S2}$$

We can express the output fields b_2, b_1 as

$$\begin{aligned} b_2 &= e^{-j\beta\ell(N-1)} a_1 + D_2 \alpha_{(1)} \ , \\ b_1 &= e^{-j\beta\ell(N-1)} a_2 + D_1 \alpha_{(2)} \ , \end{aligned} \tag{S3}$$

where the subscript of α is used only for the traveling wave resonator case. In these equations ω_0 is the resonance frequency, γ is the decay rate of the mode, and D_m is the effective coupling between port m and the resonant mode. We assume the waveguide is matched to the ports and is lossless with a propagation constant β. The couplers are spatially separated in the waveguide by a length ℓ, which leads to the term $e^{-j\beta\ell(N-1)}$ to account for the phase associated with a wave traveling between ports. At steady state the solution to equation S1 (a standing wave resonator) is

$$\alpha = \frac{D_1 a_1 + D_2 a_2}{j(\omega - \omega_0) + \gamma} \ . \tag{S4}$$

We can then rewrite equation S3 as

$$\begin{aligned} b_2 &= \left(e^{-j\beta\ell(N-1)} a_1 + \frac{D_2 D_1 a_1 + D_2 D_2 a_2}{j(\omega - \omega_0) + \gamma} \right) \ , \\ b_1 &= \left(e^{-j\beta\ell(N-1)} a_2 + \frac{D_1 D_1 a_1 + D_1 D_2 a_2}{j(\omega - \omega_0) + \gamma} \right) \ . \end{aligned} \tag{S5}$$

In the system under consideration, shown in Fig. S1, the effective coupling rates D_1 and D_2 can be written as

$$\begin{aligned} D_1 &= \sum_{n=1}^{N} j d_n e^{-j\beta\ell(n-1)} \ , \\ D_2 &= \sum_{n=1}^{N} j d_n e^{j\beta\ell(n-N)} \ , \end{aligned} \tag{S6}$$

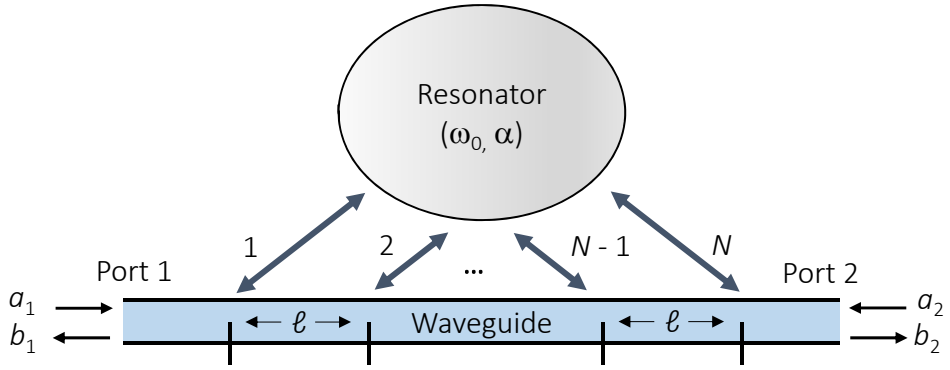

Figure S1: Schematic of a waveguide-resonator system with one resonance and two ports. The input and output at port m is described by a_m and b_m respectively and the resonant field is described by α. The ports are coupled directly via a waveguide and are also coupled to a resonant modes using a system of N spatiotemporally modulated capacitive couplers with coupling rate d_n. The individual couplers are spatially distributed over the waveguide with subwavelength spacing ℓ in order to generate sensitivity to wave propagation direction.

where we modulate the coupling rate of each individual coupler d_n with the function $d_n = d_0 + d_M \cos\big(\Omega\tau - \phi(n-1)\big)$. Under this modulation the effective coupling rates D_1 and D_2 can be expressed as

$$\begin{aligned} D_1 &= \sum_{n=1}^{N} j\left(d_0 + \frac{d_M}{2}e^{j\Omega\tau}e^{-j\phi(n-1)} + \frac{d_M}{2}e^{-j\Omega\tau}e^{j\phi(n-1)}\right)e^{-j\beta\ell(n-1)}\ , \\ D_2 &= \sum_{n=1}^{N} j\left(d_0 + \frac{d_M}{2}e^{j\Omega\tau}e^{-j\phi(n-1)} + \frac{d_M}{2}e^{-j\Omega\tau}e^{j\phi(n-1)}\right)e^{j\beta\ell(n-N)}\ . \end{aligned} \tag{S7}$$

For simplicity we assume a resonant mode with only one input ($a_1 \neq 0,\ a_2 = 0$), which could be a standing wave or traveling wave resonator. We later discuss the effects of a_2 on the standing wave case and the difference in the decay rate γ. The steady-state field in the resonator is thus

$$\begin{aligned} \alpha = {} & jd_0\frac{\sum_{n=1}^{N} e^{-j\beta\ell(n-1))}}{j(\omega-\omega_0)+\gamma}a_1 \\ & + \frac{jd_M}{2}\frac{\sum_{n=1}^{N} e^{-j(\beta\ell+\phi)(n-1)}}{j(\omega+\Omega-\omega_0)+\gamma}a_1e^{j\Omega t} \\ & + \frac{jd_M}{2}\frac{\sum_{n=1}^{N} e^{-j(\beta\ell-\phi)(n-1)}}{j(\omega-\Omega-\omega_0)+\gamma}a_1e^{-j\Omega t}\ . \end{aligned} \tag{S8}$$

The time-varying terms here represent sidebands of the resonance created by the modulated coupling, which allow waves with a frequency offset Ω from the resonance frequency to couple into the

resonance. We can now find the steady-state fields b_2 and b_1 (also with $a_2 = 0$) as

$$
\begin{aligned}
b_2 = a_1 \Bigg[& e^{-j\beta\ell(N-1)} - d_0^2 \frac{\sum_{n=1}^{N} e^{-j\beta\ell(n-1)} \sum_{m=1}^{N} e^{j\beta\ell(m-N)}}{j(\omega-\omega_0)+\gamma} \\
& - \frac{d_M^2}{4} \frac{\sum_{n=1}^{N} e^{-j\beta\ell(n-1)} e^{-j\phi(n-1)} \sum_{m=1}^{N} e^{j\beta\ell(m-N)} e^{j\phi(m-1)}}{j(\omega+\Omega-\omega_0)+\gamma} \\
& - \frac{d_M^2}{4} \frac{\sum_{n=1}^{N} e^{-j\beta\ell(n-1)} e^{j\phi(n-1)} \sum_{m=1}^{N} e^{j\beta\ell(m-N)} e^{-j\phi(m-1)}}{j(\omega-\Omega-\omega_0)+\gamma} \Bigg] \\
+ a_1 e^{\Omega t} \Bigg[& - \frac{d_0 d_M}{2} \frac{\sum_{n=1}^{N} e^{-j\beta\ell(n-1)} \sum_{m=1}^{N} e^{j\beta\ell(m-N)} e^{-j\phi(m-1)}}{j(\omega-\omega_0)+\gamma} \\
& - \frac{d_0 d_M}{2} \frac{\sum_{n=1}^{N} e^{-j\beta\ell(n-1)} e^{-j\phi(n-1)} \sum_{m=1}^{N} e^{j\beta\ell(m-N)}}{j(\omega+\Omega-\omega_0)+\gamma} \Bigg] \\
+ a_1 e^{-j\Omega t} \Bigg[& - \frac{d_0 d_M}{2} \frac{\sum_{n=1}^{N} e^{-j\beta\ell(n-1)} \sum_{m=1}^{N} e^{j\beta\ell(m-N)} e^{j\phi(m-1)}}{j(\omega-\omega_0)+\gamma} \\
& - \frac{d_0 d_M}{2} \frac{\sum_{n=1}^{N} e^{-j\beta\ell(n-1)} e^{j\phi(n-1)} \sum_{m=1}^{N} e^{j\beta\ell(m-N)}}{j(\omega-\Omega-\omega_0)+\gamma} \Bigg] \\
+ a_1 e^{2\Omega t} \Bigg[& - \frac{d_M^2}{4} \frac{\sum_{n=1}^{N} e^{-j\beta\ell(n-1)} e^{-j\phi(n-1)} \sum_{m=1}^{N} e^{j\beta\ell(m-N)} e^{-j\phi(m-1)}}{j(\omega+\Omega-\omega_0)+\gamma} \Bigg] \\
+ a_1 e^{-j2\Omega)t} \Bigg[& - \frac{d_M^2}{4} \frac{\sum_{n=1}^{N} e^{-j\beta\ell(n-1)} e^{j\phi(n-1)} \sum_{m=1}^{N} e^{j\beta\ell(m-N)} e^{j\phi(m-1)}}{j(\omega-\Omega-\omega_0)+\gamma} \Bigg] .
\end{aligned}
\tag{S9}
$$

From the output field b_2 we find the transmission coefficient $S_{21} = b_2/a_1$ (with $a_2 = 0$).

$$
\begin{aligned}
S_{21} = \Bigg[& e^{-j\beta\ell(N-1)} - d_0^2 \frac{\sum_{n=1}^{N} e^{-j\beta\ell(n-1)} \sum_{m=1}^{N} e^{j\beta\ell(m-N)}}{j(\omega-\omega_0)+\gamma} \\
& - \frac{d_M^2}{4} \frac{\sum_{n=1}^{N} e^{-j\beta\ell(n-1)} e^{-j\phi(n-1)} \sum_{m=1}^{N} e^{j\beta\ell(m-N)} e^{j\phi(m-1)}}{j(\omega+\Omega-\omega_0)+\gamma} \\
& - \frac{d_M^2}{4} \frac{\sum_{n=1}^{N} e^{-j\beta\ell(n-1)} e^{j\phi(n-1)} \sum_{m=1}^{N} e^{j\beta\ell(m-N)} e^{-j\phi(m-1)}}{j(\omega-\Omega-\omega_0)+\gamma} \Bigg] \\
+ e^{j\Omega t} \Bigg[& - \frac{d_0 d_M}{2} \frac{\sum_{n=1}^{N} e^{-j\beta\ell(n-1)} \sum_{m=1}^{N} e^{j\beta\ell(m-N)} e^{-j\phi(m-1)}}{j(\omega-\omega_0)+\gamma} \\
& - \frac{d_0 d_M}{2} \frac{\sum_{n=1}^{N} e^{-j\beta\ell(n-1)} e^{-j\phi(n-1)} \sum_{m=1}^{N} e^{j\beta\ell(m-N)}}{j(\omega+\Omega-\omega_0)+\gamma} \Bigg] \\
+ e^{-j\Omega t} \Bigg[& - \frac{d_0 d_M}{2} \frac{\sum_{n=1}^{N} e^{-j\beta\ell(n-1)} \sum_{m=1}^{N} e^{j\beta\ell(m-N)} e^{j\phi(m-1)}}{j(\omega-\omega_0)+\gamma} \\
& - \frac{d_0 d_M}{2} \frac{\sum_{n=1}^{N} e^{-j\beta\ell(n-1)} e^{j\phi(n-1)} \sum_{m=1}^{N} e^{j\beta\ell(m-N)}}{j(\omega-\Omega-\omega_0)+\gamma} \Bigg] \\
+ e^{j2\Omega t} \Bigg[& - \frac{d_M^2}{4} \frac{\sum_{n=1}^{N} e^{-j\beta\ell(n-1)} e^{-j\phi(n-1)} \sum_{m=1}^{N} e^{j\beta\ell(m-N)} e^{-j\phi(m-1)}}{j(\omega+\Omega-\omega_0)+\gamma} \Bigg] \\
+ e^{-j2\Omega t} \Bigg[& - \frac{d_M^2}{4} \frac{\sum_{n=1}^{N} e^{-j\beta\ell(n-1)} e^{j\phi(n-1)} \sum_{m=1}^{N} e^{j\beta\ell(m-N)} e^{j\phi(m-1)}}{j(\omega-\Omega-\omega_0)+\gamma} \Bigg] .
\end{aligned}
\tag{S10}
$$

The reverse transmission coefficient S_{12} can be found as $S_{12} = b_1/a_2$ (with $a_1 = 0$). We can thus understand the system as taking one input and splitting it into five frequencies separated by the

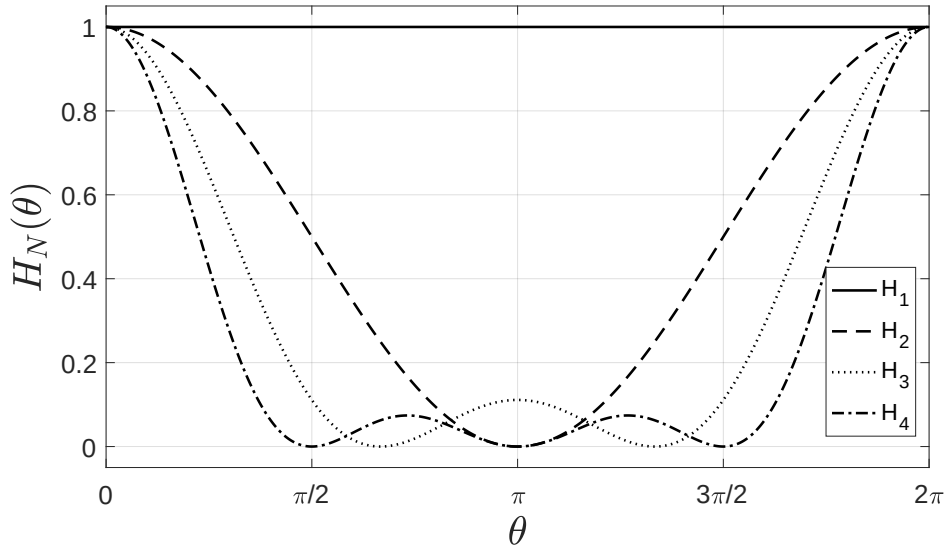

Figure S2: Plot of the coupling efficiency function $H_N(\theta)$ for $N = 1,\ 2,\ 3,\ 4$.

modulation frequency Ω. Presently, we wish to only consider the solution where output terms are the same frequency ω as the input. These are the terms that are measured on a typical network analyzer, while terms that are frequency offset can be dismissed as noise produced by the system. We then obtain

$$\begin{aligned} b_2 = a_1 \Bigg[e^{-j\beta\ell(N-1)} &- d_0^2 \frac{\sum_{n=1}^{N} e^{-j\beta\ell(n-1)} \sum_{m=1}^{N} e^{j\beta\ell(m-N)}}{j(\omega-\omega_0)+\gamma} \\ &- \frac{d_M^2}{4} \frac{\sum_{n=1}^{N} e^{-j\beta\ell(n-1)} e^{-j\phi(n-1)} \sum_{m=1}^{N} e^{j\beta\ell(m-N)} e^{j\phi(m-1)}}{j(\omega+\Omega-\omega_0)+\gamma} \\ &- \frac{d_M^2}{4} \frac{\sum_{n=1}^{N} e^{-j\beta\ell(n-1)} e^{j\phi(n-1)} \sum_{m=1}^{N} e^{j\beta\ell(m-N)} e^{-j\phi(m-1)}}{j(\omega-\Omega-\omega_0)+\gamma} \Bigg] . \end{aligned} \tag{S11}$$

Using this frequency limited output we can rewrite S_{21} as

$$\begin{aligned} S_{21} = e^{-j\beta\ell(N-1)} \Bigg[1 &- \frac{d_0^2 N^2 H_N(\beta\ell)}{j(\omega-\omega_0)+\gamma} - \frac{1}{4} \frac{d_M^2 N^2 H_N(\beta\ell+\phi)}{j(\omega+\Omega-\omega_0)+\gamma} \\ &- \frac{1}{4} \frac{d_M^2 N^2 H_N(\beta\ell-\phi)}{j(\omega-\Omega-\omega_0)+\gamma} \Bigg] . \end{aligned} \tag{S12}$$

We have introduced the coupling efficiency function

$$H_N(\theta) = \frac{1}{N^2} \left| \sum_{n=1}^{N} e^{-j\theta n} \right|^2 . \tag{S13}$$

The function $H_N(\theta)$ is a periodic even function that is symmetric about $\theta = n\pi$ for integer n as illustrated in Fig. S2 for selected values of N.

While the above derivation assumes $a_2 = 0$, this system can be readily solved for simultaneous inputs a_1 and a_2 as written in equations S1 and S3. It is clear from equation S4 that for a standing wave resonator the resonant field α is simply a superposition of the contribution from both inputs,

therefore in general the outputs b_1 and b_2 depend on both inputs. This dependence is obviously undesirable for the functionality of a system but is resolved in the case where waves propagating in one direction are completely uncoupled from the resonance (completely unidirectional coupling). As discussed in the manuscript this condition is also important to other functions of the system such as lossless functionality and isolation. The dependence of the outputs on both inputs is automatically resolved for a traveling wave resonator since the orthogonal resonant fields each only depend on one of the inputs.

S2 Derivation of the decay rate

As previously shown[24], the decay rate γ for a lossless resonator is defined as

$$2\gamma = D_1 D_1^* + D_2 D_2^* \tag{S14}$$

which can be extended to lossy resonators through the addition of the intrinsic decay rate κ_i. We note that for a traveling wave resonance only the D term coupling the resonant field to the output field b (in equation S3) is used. Our system has time-varying D_m, so is it necessary to slightly modify this definition to

$$2\gamma = \langle D_1 D_1^* + D_2 D_2^* + \kappa_i \rangle \tag{S15}$$

where $\langle\ \rangle$ represents the time-average. This approximation is valid because $\gamma << \Omega$ and the field in the resonator decays very slowly compared to the modulation. The expression for γ can then be simplified to

$$\begin{aligned} 2\gamma = {} & 2d_0^2 N^2 H_N(\beta_\omega \ell) \\ & + \frac{1}{4} d_M^2 N^2 H_N(\beta_{\omega-\Omega}\ell + \phi) + \frac{1}{4} d_M^2 N^2 H_N(\beta_{\omega+\Omega}\ell - \phi) \\ & + \frac{1}{4} d_M^2 N^2 H_N(\beta_{\omega+\Omega}\ell + \phi) + \frac{1}{4} d_M^2 N^2 H_N(\beta_{\omega-\Omega}\ell - \phi)\ , \end{aligned} \tag{S16}$$

where the frequency dependence of β is explicitly written for clarity. The decay rate γ defines the resulting modal linewidth and is present in the denominator of all the S-parameter equations for our nonreciprocal time-varying coupler.

References

[1] Strutt, J. W. Some general theorems relating to vibrations. *Proceedings of the London Mathematical Society* **4**, 357–368 (1873).

[2] Jalas, D. *et al.* What is - and what is not - and optical isolator. *Nature Photonics* **7**, 579–582 (2013).

[3] Maznev, A. A., Every, A. G. & Wright, O. B. Reciprocity in reflection and transmission: What is a 'phonon diode'? *Wave Motion* **50**, 776–784 (2013).

[4] Hogan, C. L. The ferromagnetic Faraday effect at microwave frequencies and its applications - the microwave gyrator. *The Bell System Technical Journal* **31**, 1–31 (1952).

[5] Jin, J.-M. *Theory and Computation of Electromagnetic Fields* (John Wiley and Sons, Hoboken, New Jersey, 2010).

[6] Casimir, H. B. G. Reciprocity theorems and irreversible processes. *Proceedings of the IEEE* **51**, 1570–1573 (1963).

[7] Yu, Z. & Fan, S. Complete optical isolation created by indirect interband photonic transisions. *Nature Photonics* **3**, 91–94 (2008).

[8] Kamal, A., Clarke, J. & Devoret, M. H. Noiseless non-reciprocity in a parametric active device. *Nature Physics* **7**, 311–315 (2011).

[9] Hafezi, M. & Rabl, P. Optomechanically induced non-reciprocity in microring resonators. *Optics Express* **20**, 7672–7684 (2012).

[10] Lira, H., Yu, Z., Fan, S. & Lipson, M. Electrically drive nonreciprocity induced by interband photonic transition on a silicon chip. *Physical Review Letters* **109**, 033901 (2012).

[11] Fang, K., Yu, Z. & Fan, S. Photonic Aharonov-Bohm effect based on dynamic modulation. *Physical Review Letters* **108**, 153901 (2012).

[12] Fang, K., Yu, Z. & Fan, S. Experimental demonstration of a photonic Aharonov-Bohm effect at radio frequencies. *Physical Review B* **87**, 060301 (2013).

[13] Estep, N. A., Sounas, D. L., Soric, J. & Alu, A. Magnetic-free non-reciprocity and isolation based on parametrically modulated coupled-resonator loops. *Nature Physics* **10**, 923–927 (2014).

[14] Fleury, R., Sounas, D. L., Sieck, C. F., Haberman, M. R. & Alu, A. Sound isolation and giant linear nonreicprocity in a compact acoustic circulator. *Science* **343**, 516–519 (2014).

[15] Tzuang, L. D., Fang, K., Nussenzveig, P., Fan, S. & Lipson, M. Non-reciprocal phase shift induced by an effective magnetic flux for light. *Nature Photonics* **8**, 701–705 (2014).

[16] Qin, S., Xu, Q. & Wang, Y. E. Nonreciprocal components based on distributed modulated capacitors. *IEEE Transactions on Microwave Theory and Techniques* **62**, 2260–2272 (2014).

[17] Kim, J., Kuzyk, M. C., Han, K., Wang, H. & Bahl, G. Non-reciprocal Brillouin scattering induced transparency. *Nature Physics* **11**, 275–280 (2015).

[18] Dong, C.-H. *et al.* Brillouin-scattering-induced transparency and non-reciprocal light storage. *Nature Communications* **6**, 6193 (2015).

[19] Estep, N. A., Sounas, D. L. & Alu, A. Magnetless microwave circulators based on spatiotemporally modulated rings of coupled resonators. *IEEE Transactions on Microwave Theory and Techniques* **64**, 502–518 (2016).

[20] Reiskarimian, N. & Krishnaswamy, H. Magnetic-free non-reciprocity based on staggered commutation. *Nature Communications* **7**, 11217 (2016).

[21] Shen, Z. *et al.* Experimental realization of optomechanically induced non-reciprocity. *Nature Photonics* **10**, 657–661 (2016).

[22] Haus, H. *Waves and Fields in Optoelectronics* (Prentice-Hall, Englewood Cliffs, New Jersey, 1984).

[23] Fan, S., Suh, W. & Joannopoulos, J. D. Temporal coupled-mode theory for the Fano resonance in optical rsonators. *J. Opt, Soc. Am. A* **20**, 569–572 (2003).

[24] Suh, W., Wang, Z. & Fan, S. Temporal coupled-mode theory and the presence of non-orthogonal modes in lossless multimode cavities. *IEEE Journal of Quantum Electronics* **40**, 1511–1518 (2004).

[25] Yu, C.-C. & Chang, K. Transmission-line analysis of a capacitively coupled microstrip-ring resonator. *IEEE Transactions on Microwave Theory and Techniques* **45**, 2018–2024 (1996).

[26] Kang, M. S., Butsch, A. & Russell, P. S. J. Reconfigurable light-driven opto-acoustic isolators in photonic crystal fibre. *Nature Photonics* **5**, 549–553 (2011).